Synthetic biosensor circuits generate a frequency-encoded response to phytohormones under a dynamic environment

S. Pérez García[1,†], M. García Navarrete[1,†], D. Ruiz Sanchis[1], C. Prieto Navarro[1], M. Avdovic[1], O. Pucciariello[1], K. Wabnik[1,*]

[1]Centro de Biotecnologıa y Genomica de Plantas (Universidad Politecnica de Madrid – Instituto Nacional de Investigacion y Tecnologıa Agraria y Alimentaria), Autopista M-40, Km 38 – 28223 Pozuelo de Alarcon, Spain

*Correspondence to: k.wabnik@upm.es

†Contributed equally.

Summary

Phytohormones auxin and salicylic acid (SA) are tiny signaling molecules with tremendous importance to plants. Neither direct nor orthogonal signaling systems that combine these hormones exist. Here, we designed and implemented compact synthetic gene circuits for direct sensing of auxin and SA by hijacking multiple antibiotic resistance proteins from bacteria. Using all-atom modeling, time-lapse live cell imaging, and microfluidics we demonstrated that these synthetic biosensors respond to physiological concentrations of hormones with a near-linear precision while offering memory of previous hormone states. By coupling biosensors, we constructed a synthetic phytohormone crosstalk system capable of converting the frequency of hormone stimulus to the speed of the circuit response in a dynamically changing environment generated on the microfluidic chip. Our approach provides a simple, yet powerful tool for exploring phytohormone distribution dynamics and designing complex regulatory modules that turn dynamic environmental cues into precise response times.

Plants show remarkable potential for adaption to the environment by maintaining a tight balance between growth and immune responses[1,2]. Small molecules auxin and salicylic acid (SA) carry information about environmental changes to downstream regulatory networks that tailor plant body architecture[3-8]. This ability to respond to auxin and SA was also a key innovation in the evolution of land plants that enabled the terrestrial colonization[9]. However, the quantitative tracking of auxin and salicylic acid remains very challenging[10-13]. Existing biosensors for auxin and SA are non-direct, irreversible, and lack a linear dynamic range[14] which impedes the quantitative tracking of phytohormone signaling dynamics[15], and hampers biotechnological applications. Thus, an increasing demand for direct biosensors for auxin and SA embedded in orthogonal signaling systems, creates opportunities for the exploration of the microbial world (recent preprint: Herud-Sikimic, O., et al, (2020), https://doi.org/10.1101/2020.01.19.911735), in the search for intermediate solutions.

Several soil-associated microbes evolved a profound capacity for sensing and metabolizing phenolic compounds such as SA to control stress and fitness responses[16,17]. Here, we focused on the family of multiple antibiotic resistance (Mar) proteins that sense selectively, a myriad of phenolic compounds in the environment[18,19]. *E.coli* MarR transcriptional repressor is a representative member of this family that controls a microbial antibiotic stress response to salicylate (Supplementary Fig.1)[20,21]. However, it is mechanistically unclear how phenolic agents such as SA regulate MarR repressors activity[19,20].

Here, we identified and implemented compact, direct synthetic sensors for auxin and SA by hijacking the MarR transcriptional repressors. These biosensor circuits robustly respond to hormones with near-linear dynamic range, and could be combined to program sophisticated regulatory functions including logic gating and frequency-encoded response to detected changes of hormone levels in the environment.

We initially address the elusive dynamics of ligand sensing by MarR repressors with all-atom molecular dynamics (MD) simulations on MarR crystal structures. MD simulations demonstrate that MarR apoprotein remained flexible (Fig. 1a) and adapt to the shape of the DNA operator by adjusting a distance between DNA binding (DB) domains (Fig. 1a and Supplementary Fig. 2a, Supplementary Movies 1 and 2). On the contrary, the presence of SA in the MarR dimerization interface brought monomers close to each other, creating a rigid closed structure (Fig. 1b, Supplementary Movie 3) unable to bind DNA. We then calculated the

probability distribution of the distance between R73 residues of DB domains that are in direct contact with nucleic bases (Fig. 1c). We found that only apoprotein, largely due to its flexibility (Supplementary Fig. 2b), was able to scan across various distances and eventually sat at the DNA-bound state (Fig. 1c). To address the dynamics of conformation changes, we performed the metadynamics energy landscape analysis with the local perturbation of distance between R73 atoms of both monomers (see Supplementary Information for details).

Time-dependent changes of energy portraits in apoprotein and DNA-bound MarR configurations revealed the presence of a stable energy minimum (M), which was absent in holoprotein simulations (Fig. 1d). This minimum corresponds to the smallest deviation from the reference distance of ≈ 20 A˚ between DB domains, as observed in crystals of DNA-bound MarR (Supplementary Fig. 2a). Collectively, our findings indicate that MarR repressor requires high flexibility to adapt to DNA operator sites which, is negatively regulated by phytohormone exposure.

Several homologs of MarR repressors recognize other phenolic-based compounds[18-21]. Among those, the IacR from *A. Baumanii* is sensitive to naturally occurring auxin such as 3-indoleacetic acid (IAA)[22,23]. Next, we asked if iacR could respond to auxin using a similar mechanism to that of MarR. The model of iacR predicted that apoprotein remains flexible concerning the spacing between DB domains (Supplementary Fig. 3a). In contrast, the bound IAA stretched the distance between DB domains (Supplementary Fig. 3b,c), as demonstrated by the distance distribution between DB domains (Supplementary Fig. 4a) and metadynamics analysis (Supplementary Fig. 4b). Therefore predicted iacR dynamics share common design principles of DNA recognition with MarR, including backbone flexibility and successive switches of conformation state.

The *S. cerevisiae* serves the eukaryotic chassis for synthetic biology applications. To test putative biosensors in this eukaryotic host, we fused MarR or IacR with a strong herpes simplex virus trans-activation domain (VP64)[24] under the galactose-induced promoter (Fig. 2a,b and Supplementary Fig. 5a). Also, we tagged MarR-type biosensors with mouse ornithine decarboxylase (ODC) degron[25] for fast degradation dynamics. To report circuit response, we used a Green fluorescent reporter (dEGFP) expressed from the synthetic minimal promoter with putative MarR[19] or IacR operator sequences[23], also tagged with uncleavable ubiquitin (G76V mutant)[26] at the N-terminus for fast degradation (Fig. 2a,b and Supplementary Fig. 5a). We

found that IacR-VP64 could robustly respond to a stable concentration gradient of IAA with an excellent detection limit towards the nM range (Supplementary Fig. 6a). Similarly, MarR-VP64 responded to the linear SA gradient, however higher SA concentrations (μM range) were effective in the significant reduction of reporter levels (Supplementary Fig. 6b).

To further characterize the dynamics of MarR-type biosensors, we tested the circuit response in a dynamic environment that is governed by transient changes in auxin and SA levels. For that purpose, we applied and customized rapid, cost-effective lithography technologies[27] for the fabrication of microfluidic devices (see Supplementary Fig. 7 and Supplementary Information for details). Microfluidics chip integrates a time-dependent switching of two independent media inputs, through a chaotic mixer module (Supplementary Fig. 8a,b). To resolve the dynamics of biosensors, we performed a chaotic microfluidic mixing with a linear decrease and subsequent increase of auxin and SA in 10-hour cycles to mimic a linear concentration gradient (Fig. 2c,d). Notably, we could observe, in our microfluidic experiments, a prominent pulse of reporter gene dEGFP synchronized in the populations of exponentially growing cells across traps (Fig. 2e-g, Supplementary Movies 4 and 5). These pulses are reminiscent of analogous cycles of charging and discharging of a capacitor (Fig. 2c,d). We speculate that this ’capacitance’ reflects the degree of the structural rigidity of MarR-type repressors correlated with ligand binding events (Fig. 1b, Supplementary Movie 3). Thus, we concluded that unlike previous biosensors, MarR-type biosensors act as biological ’capacitors’ for auxin and SA, displaying a near-linear response to hormone concentration changes.

Auxin and SA crosstalk on multiple levels, including transcriptional and posttranslational regulation of plant development and adaptation to the environment[28]. A successful assembly of synthetic orthogonal crosstalk of phytohormones was never been achieved before. Thus, we attempted to combine our auxin and SA biosensor circuits to construct synthetic, orthogonal crosstalk to which we refer as 'CrossTalker' (Fig. 3a). The general scheme of this synthetic module includes the IacR-VP64 activator and MarR repressor directly fused to the repression domain from yeast MIG1 transcriptional regulator[29] (Fig. 3a and Supplementary Fig. 5b). The CrossTalker displayed a robust graded response to step-wise elevations of both phytohormones in multiwell plate fluorescence scanning assays (Supplementary Fig. 9a). We performed time-lapse microscopy with alternating input conditions for IAA and SA, and we could observe the gated response, reassembling the NIMPLY logic gate (Supplementary Fig. 9b). These results

confirm that the synthetic crosstalk device is capable of responding to dynamic concentration gradients.

The reconstitution of *in vivo* hormone gradients in laboratory conditions is far from trivial task. However, our microfluidic platform provides hormone mixing over the time course of the experiment, producing alternating gradients of auxin and SA. For that purpose, we used a double spike generator shifted in phase by π with a period of 10 hours, consistent with the previous experiment (see Supplementary Information for further details). We found that the CrossTalker circuit (Fig. 3a) exhibited dynamic waves of reporter gene expression (Fig. 3b,c, Supplementary Movie 6). Reporter peaks were separated by approximately three periods of an input signal (Fig. 3d and Supplementary Fig. 9c) with the negligible variation in peak amplitudes (Supplementary Fig. 9d). To further understand the cause of a delay between consecutive peaks observed in experiments we constructed a computer model of hormone crosstalk (Supplementary Fig. 10a-c, see SI for model description). We found that a model with a delay in the repression (MarR-RD) could produce a similar output (Supplementary Fig. 10c) to that observed experimentally (Fig. 3b). Thus, these findings from computer model simulations are in good agreement with the observations of a delayed MarR response to changes in phytohormone compared to that of IacR sensor (Fig. 2c,d).

Finally, we tested whether increasing the frequency of stimulus could lead to an increased speed of CrossTalker responsiveness, providing the frequency entrainment mechanism (Fig. 3e). First, we simulated our model with 5-hour repetitive anti-phase pulses of SA and IAA. The computer model simulations of the CrossTalker circuit predict a correct synchronization with the cyclic phytohormone stimulus (Supplementary Fig. 10d). These predictions from the computer model reveal the hormone 'capacitance' may change with the frequency of the stimulus, allowing the fast adaptation to the environmental conditions. We tested this intriguing theory on a microfluidic chip by subjecting the Crosstalker circuit to 5-hour pulses of IAA and SA (Fig. 3f). The time-lapse live yeast imaging in microfluidic traps revealed robust, synchronized oscillations of a reporter gene (Fig. 3f,g, Supplementary Movie 7) with a mean period of 5 hours (Fig. 3h) and minimal variation of the amplitude (Supplementary Fig. 11a). Furthermore, experiments demonstrate a time-dependent increase in the period of oscillations (phase diffusion) at the colony level (Supplementary Fig. 11b). Consistently, we could observe two eminent synchronization modes 1:1 and 1.5:1 in our experiments (Supplementary Fig. 11c). These data

indicate that CrossTalker device senses dynamic fluctuations in the environment and respond with increased speed and precision by decoding the frequency of hormone input cycles. Thus, our data pinpoint requirements for a minimal, phytohormone cross-talk circuit that is robust and capable of an adaptive response to the surrounding environment.

Here, we have implemented and characterized minimal biosensors for auxin and SA based solely on bacterial antibiotic resistance proteins. By combining structural insights, computer modeling, and microfluidics, we demonstrated these biosensors robustly sense physiological hormone concentrations. Synthetic circuits were tested in yeast in the precisely controlled environment to reveal a near-linear dynamic characteristics. Thus, proposed biosensors offer vast opportunities for direct tracking of phytohormone distribution across time and space through the interface with the environment. Furthermore, we introduced the concept of synthetic phytohormone crosstalk which offers means for the precise adjustment of response speed according to frequencies of exogenous hormone stimulus. As such this hormone crosstalk device provides an efficient decoding scheme for interpreting rapid hormone changes.

In summary, our study provides an important step forward towards quantitative monitoring of plant hormone distribution dynamics as well as future biotechnological applications such as the construction of synthetic phytohormone signaling circuits in both plants and plant-associated microorganisms.

.

References

1. M. Naseem et al., The nexus between growth and defense signalling: Auxin and cytokinin modulate plant immune response pathways. *Journal of experimental botany* **66** (2015).

2. A. Robert-Seilaniantz, et al., Hormone Crosstalk in Plant Disease and Defense: More Than Just JASMONATE-SALICYLATE Antagonism. *Annual Review of Phytopathology* **49**, 317–343 (2011).

3. M. Lavy & M. Estelle., Mechanisms of auxin signaling. *Development* **143**, 3226–3229 (2016).

4. D. Weijers & D. Wagner., Transcriptional Responses to the Auxin Hormone. *Annual review of plant biology* **67**, 539–574 (2016).

5. D. Kumar., Salicylic acid signaling in disease resistance. *Plant science : an international journal of experimental plant biology* **228**, 127–134 (2014).

6. A. C. Vlot et al., Salicylic Acid, a multifaceted hormone to combat disease. *Annual review of phytopathology* **47**, 177–206 (2009).

7. S. Tan et al., Salicylic Acid Targets Protein Phosphatase 2A to Attenuate Growth in Plants. *Current Biology*, **30** (2020).

8. T. Pasternak et al., Salicylic Acid Affects Root Meristem Patterning via Auxin Distribution in a Concentration-Dependent Manner. *Plant Physiology* **180**, 1725-1739 (2019).

9. M. A. Blazquez et al., Evolution of plant hormone response pathways. *Annual Review of Plant Biology* **71**, (2020).

10. G. Brunoud et al., A novel sensor to map auxin response and distribution at high spatio-temporal resolution. *Nature* **482**, 103–106 (2012).

11. C.-Y. Liao et al., Reporters for sensitive and quantitative measurement of auxin response. *Nature Methods* **12**, 207–210 (2015).

12. W. E. Huang et al., Quantitative *in situ* assay of salicylic acid in tobacco leaves using a genetically modified biosensor strain of *Acinetobacter sp*. ADP1. *The Plant Journal* **46**, 1073–1083 (2006).

13. C. T., Defraia et al., A rapid biosensor-based method for quantification of free and glucose-conjugated salicylic acid. *Plant methods* **4**, 28 (2008).

14. B. Parızkova et al., What Has Been Seen Cannot Be Unseen - Detecting Auxin In Vivo. *International Journal of Molecular Sciences* **18**, 2736 (2017).

15. A. Larrieu et al., Comparison of plant hormone signalling systems. *Essays in Biochemistry* **58**, 165–181 (2015).

16. G. A. Beggs et al., MarR family proteins are important regulators of clinically relevant antibiotic resistance. *Protein science* **29**, 647–653 (2020).

17. S. P. Wilkinson et al., Ligand-responsive transcriptional regulation by members of the MarR family of winged helix proteins. *Current issues in molecular biology* **8**, 51–62 (2006).

18. D. K. Deochand et al., MarR family transcription factors: dynamic variations on a common scaffold. *Critical reviews in biochemistry and molecular biology* **52**, 595–613 (2017).

19. M. N. Alekshun et al., The crystal structure of MarR, a regulator of multiple antibiotic resistance, at 2.3 A resolution. *Nature structural biology* **8**, 710–714 (2001).

20. Z. Hao et al., The multiple antibiotic resistance regulator MarR is a copper sensor in Escherichia coli. *Nature chemical biology* **10**, 21–28 (2014).

21. I. C. Perera et al., MarR homologs with urate-binding signature. *Protein science* **20**, 621–629 (2011).

22. J. C. Scott et al., Functional characterization of the bacterial iac genes for degradation of the plant hormone indole-3-acetic acid. *Journal of chemical ecology* **39**, 942–951 (2013).

23. H.-Y. Shu et al., Transcriptional regulation of the iac locus from Acinetobacter baumannii by the phytohormone indole-3-acetic acid. *Antonie van Leeuwenhoek* **107**, 1237–1247 (2015).

24. K. Seipel et al., Different activation domains stimulate transcription from remote ('enhancer') and proximal ('promoter') positions. *The EMBO Journal* **11**, 4961– 4968 (1992).

25. J. Takeuchi et al., Structural elements of the ubiquitin-independent proteasome degron of ornithine decarboxylase. *Biochemical Journal* **410**, 401– 407 (2008).

26. J. H. Stack et al., A ubiquitin-based tagging system for controlled modulation of protein stability. *Nature Biotechnology* **18**, 1298–1302 (2000).

27. A. Grimes et al., Shrinky-Dink microfluidics: rapid generation of deep and rounded patterns. *Lab on a Chip* **8**, 170–172 (2008).

28. C. S. Westfall et al., *Arabidopsis thaliana* GH3.5 acyl acid amido synthetase mediates metabolic crosstalk in auxin and salicylic acid homeostasis. *Proceedings of the National Academy of Sciences* **113**, (2016).

29. J., Ostling et al., Functional domains in the Mig1 repressor. *Molecular and Cellular Biology* 1**6**, 753 LP – 761 (1996).

30. D. G. Gibson et al., Enzymatic assembly of DNA molecules up to several hundred kilobases. *Nature Methods* **6**, 343–345 (2009).

Acknowledgments: We are grateful to L. Rubio for sharing yeast strain CEN.PK2-1C. Authors thank Mark Estelle for critical discussions at the early stage of the project. This work was supported by the Programa de Atraccion de Talento 2017 (Comunidad de Madrid, 2017-T1/BIO-5654 to K.W.), Severo Ochoa (SO) Programme for Centres of Excellence in R&D from the Agencia Estatal de Investigacion of Spain (grant SEV-2016-0672 (2017-2021) to K.W. via the CBGP). In the frame of SEV-2016-0672 funding M.A. received a PhD fellowship (SEV-2016-0672-18-3: PRE2018-084946) and O.P. is supported with a postdoctoral contract. K.W. was supported by Programa Estatal de Generacion del Conocimiento y Fortalecimiento Cientıfico y Tecnologico del Sistema de I+D+I 2019 (PGC2018-093387-A-I00) from MICIU (to K.W.).

Author contributions: S.P.G and M.G.N designed, performed most of experiments and analyzed data. D.R.S, C.P.N and O.P contributed to plasmid and strain constructions, S.P.G and M.A, performed multi-well plate fluorescence assays. M.G.N performed microfluidics experiments. K.W designed experiments analyzed data and supervised the project. All authors contribute to the manuscript writing.

Competing interests: Authors declare no competing interests.

Data and materials availability: All data that support the findings of this study are available in the manuscript. Original data that supports the findings are available from the corresponding author upon request. Plasmids sequences will be deposited in NCBI database after publication. Correspondence and requests for materials such as should be addressed to K.W. (k.wabnik@upm.es). Image processing and analysis were performed using Fiji (v.1.0) and Matlab (R2018b) and R-studio. Subsequent analysis was performed using custom R and Matlab scripts. The codes are available upon request from the corresponding author.

Supplementary Information contains:

Description of methods

Supplementary Figures 1-11

Supplementary Movies 1-7

Figures

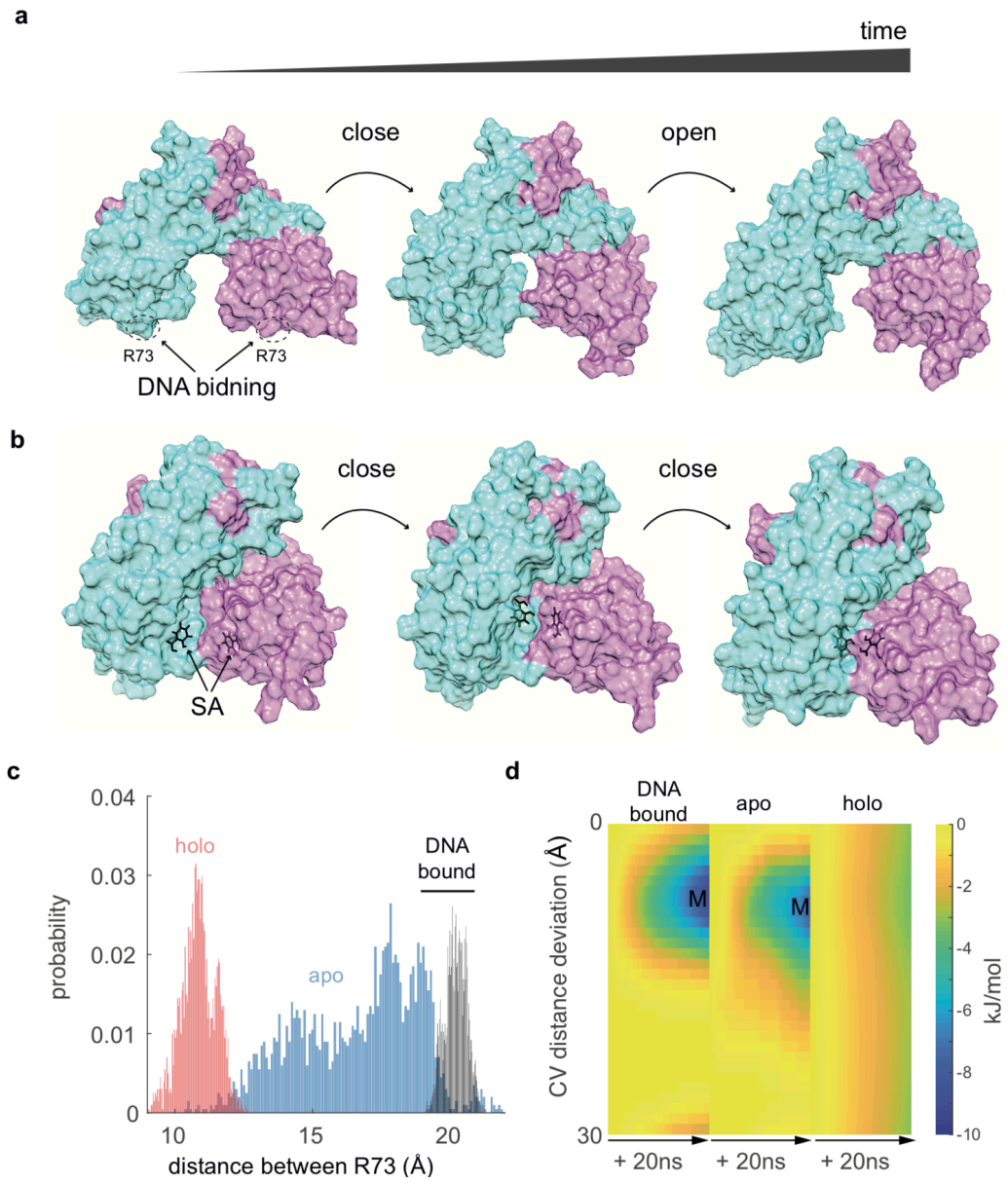

Fig. 1. Similarities in structure and mechanism of phytohormone sensing through MarR-type regulators.

(**a, b**), Time-lapse from Molecular Dynamics Simulations of the flexible MarR apoprotein (monomers are shown in cyan and purple) (a) (RCSB: 5h3r and 3voe) display a cyclic change of conformation states (open-closed-open). (b), MarR bound to two molecules of SA (black, RCSB: 1jgs) display successive shortening of the distance between R73 that reflects an unbinding of

MarR from DNA. (**c**), A probability distribution of the mean distance between R73 atoms of both monomers for apo (blue), holo(red), and DNA-bound (black) configurations. Note that the holo state provides a ≈ 2-fold short distance between DBD domains than that required for a stable bond with DNA. (**d**), Energy landscapes for three MarR configurations (apo, holo, DNA-bound) for deviation from the preferred distance of ≈ 20 A˚between R73 (both chains) required for DNA binding. Note energy minima wells (M) for apo and DNA bound configurations which were absent in holoprotein simulations indicating that the hormone-bound MarR did not reach an energy minimum required for the association with the DNA.

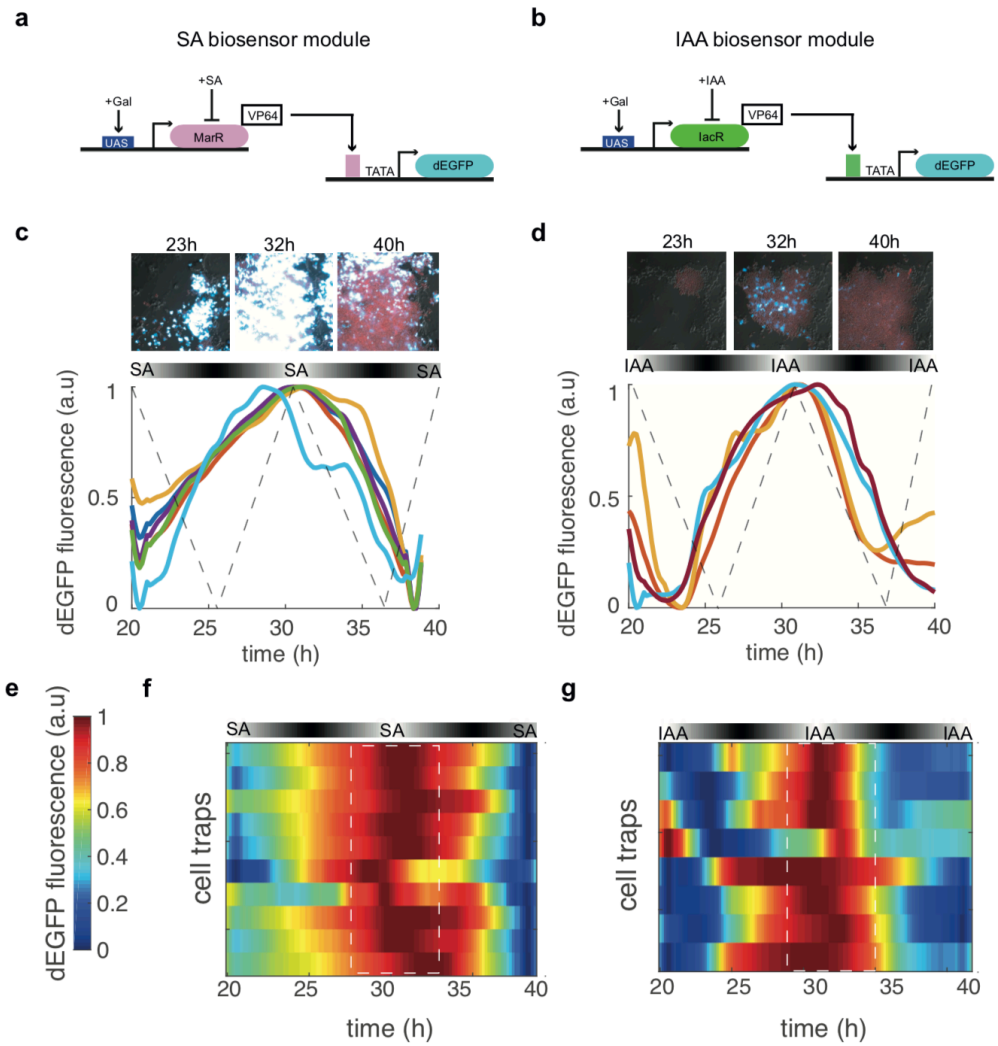

Fig. 2. Biosensor circuits show a high dynamic range in response to linear concentration gradients of phytohormones.

(**a, b**), Schematics of SA (a) and IAA (b) biosensor circuits. MarR or IacR repressors are tagged with a synthetic VP64 viral transactivation domain, nuclear localization signal (NLS), and ODC degron. Galactose is used to induce the transcription of biosensors. The fluorescent reporter (dEGFP) contains an uncleavable ubiquitin (G76V) tagged to N-terminus of enhanced GFP (EGFP) that is driven by the minimal promoter with either MarR(pink bar) or IacR(green bar) operators placed directly upstream of TATA-box. (**c-e**), Examples of screenshots and plots from time-lapse experiments on a microfluidic device with linear gradients of phytohormones (dashed lines). Three channels were simultaneously imaged using Differential interference contrast (DIC), dEGFP (cyan), and mCherry settings. Constitutive mCherry fluorescence was observed in

exponentially growing cells. dEGFP was normalized between 0 and 1 (e). Cells transformed with MarR biosensor circuit (c) displayed a broader peak and slower response to a cyclic linear change in hormone concentrations (10 hours period of SA or IAA) compared to cells equipped with the synthetic auxin sensor (d). Both circuits show a robust dynamic response to alterations in hormone concentrations as manifested by near-linear rise and fall of the reporter signal. (**f, g**), Heat maps of normalized mean dEGFP fluorescence for each trap on microfluidics device with SA (f) or IAA (g) biosensor circuits, related to (c) and (d).

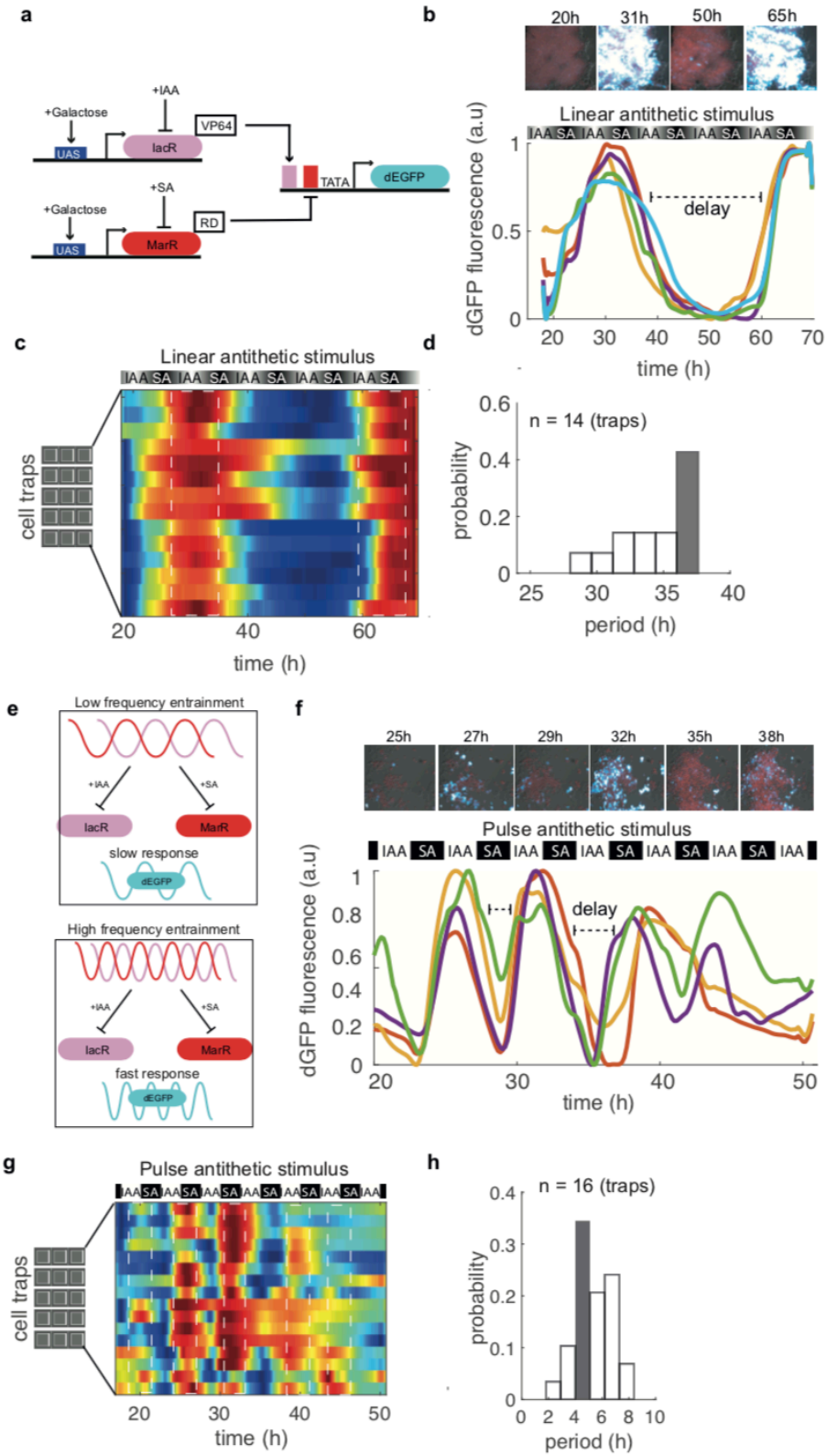
a
+Galactose
+IAA
VP64
UAS
lacR
TATA
dEGFP
+Galactose
+SA
RD
UAS
MarR
b
20h
31h
50h
65h
Linear antithetic stimulus
IAA SA IAA SA IAA SA IAA SA IAA SA
dGFP fluorescence (a.u)
delay
time (h)
c
Linear antithetic stimulus
IAA SA IAA SA IAA SA IAA SA IAA SA
cell traps
time (h)
d
n = 14 (traps)
probability
period (h)
e
Low frequency entrainment
+IAA
+SA
lacR
MarR
slow response
dEGFP
High frequency entrainment
+IAA
+SA
lacR
MarR
fast response
dEGFP
f
25h
27h
29h
32h
35h
38h
Pulse antithetic stimulus
IAA SA IAA SA IAA SA IAA SA IAA SA IAA SA IAA
dGFP fluorescence (a.u)
delay
time (h)
g
Pulse antithetic stimulus
IAA SA IAA SA IAA SA IAA SA IAA SA IAA SA IAA
cell traps
time (h)
h
n = 16 (traps)
probability
period (h)

Fig. 3. CrossTalker circuit response adapts to the dynamic environment through the frequency-entrainment mechanism.

(**a**), Implementation of the CrossTalker circuit. MarR was tagged with the repression domain consisting of the last 24 amino acids of MIG1 transcriptional repressor, nuclear localization signal (NLS), and mouse ODC degron and combined with activating IacR-VP64-ODC construct. A synthetic promoter that drives dEGFP, consists of IacR and MarR operators upstream of TATA-box. (**b, c**), Examples of CrossTalker circuit dynamics in cells that were grown in the microfluidic device with 10-hour antithetic waves of SA and IAA. Note delayed peaks of reporter gene expression (b) that were consistently synchronized across all trapping regions (c). Heat color maps are as in Fig. 2e. (**d**), A histogram of mean period distribution from traps on the microfluidics chip. Gray bar show a dominant frequency of response. (**e**), A cartoon demonstrates the principles of frequency entrainment mechanism for the Crosstalker circuit. For slow cycles of the input stimulus, a circuit displays a slow response (upper panel). Increased frequency of the stimulus is decoded by the circuit to adjust the speed of response (lower panel). (**f, g**), Dynamics of crosstalk circuit response towards the increased frequency of antithetic hormone stimulus (f) show a good synchronization across traps at the colony level (g), revealing frequency-dependent tunability of the CrossTalker circuit. (**h**), A period probability distribution displays a dominant frequency (gray bar) of response locked to the input signal frequency.